Rational Co-Design of Polymer Dielectrics for Energy Storage

*Arun Mannodi-Kanakkithodi, Gregory M. Treich, Tran Doan Huan, Rui Ma, Mattewos Tefferi, Yang Cao, Gregory A. Sotzing, and Rampi Ramprasad**

Although traditional materials discovery has historically benefited from intuition-driven experimental approaches and serendipity, computational strategies have risen in prominence and proven to be a powerful complement to experiments in the modern materials research environment. It is illustrated here how one may harness a rational co-design approach—involving synergies between high-throughput computational screening and experimental synthesis and testing—with the example of polymer dielectrics design for electrostatic energy storage applications. Recent co-design efforts that can potentially enable going beyond present-day "standard" polymer dielectrics (such as biaxially oriented polypropylene) are highlighted. These efforts have led to the identification of several new organic polymer dielectrics within known generic polymer subclasses (e.g., polyurea, polythiourea, polyimide), and the recognition of the untapped potential inherent in entirely new and unanticipated chemical subspaces offered by organometallic polymers. The challenges that remain and the need for additional methodological developments necessary to further strengthen the co-design concept are then presented.

1. Introduction

Scientific discoveries and technological innovations have benefited enormously from seemingly "trial and error" practices, and serendipity. A classic example that is often quoted in this context is the work of Thomas Edison surrounding the discovery of suitable materials for the light-bulb filament.[1,2] Although the "Edisonian Approach" has been replicated time and time again in materials science and related fields by systematically (and laboriously) experimenting on several candidate materials,[3–5] recent materials discovery efforts approach this problem in a more rational manner using computations in the first screening stage (and in subsequent steps as required).[6] The initial down-selection effort based on advanced computations, when combined with targeted additional computations, materials synthesis, testing and validation, is referred to here as "co-design". This emerging rational materials co-design paradigm can significantly reduce costs, provide enormous insights, and speed up the materials design process.

For the rational computation-guided co-design approach to work—at least in the manner practiced in the recent past—the problem has to be amenable to rapid high-throughput computations, and it should be possible to state the (initial) screening criteria in terms of calculable properties. If such is the case, the "domain experts" of the materials and applications subfields frame the chemical subspace to be explored defined by the atoms/structural units and the framework in which such units may be placed; this will lead to a list of combinatorial possibilities. Additionally, the domain experts specify computable properties that are relevant to the desired application. High-throughput computations are then performed on these systems, at a chosen acceptable level of theory, to determine the properties deemed important in the initial screening step, leading to a shortlist of potentially useful candidate materials. Following this, the materials synthesis specialist further reduces the shortlist by determining which cases would be amenable to synthesis, considering both the availability of starting materials and the cost of production. Only at this point are any benchtop experiments done, and attempts are made to produce the few selected materials. Those successfully synthesized undergo in-depth computations to include additional details previously ignored during the initial high-throughput screening step (such as the actual crystal structure or morphology, requirement of a higher level of theory for some properties, etc.). The computed results are then compared with measurement results for validation, and the results are analyzed. Further in-depth studies are planned that may lead to an alteration of the initial chosen chemical subspace, and the process may continue in an iterative manner. A possible workflow that captures these notions is portrayed in **Figure 1**.

The successes of such efforts over the last few years were recently reviewed.[7] Notable examples of computation-guided discoveries include the identification of new cathode materials for Li-ion batteries,[8] design of Li-doped Cr_2MnO_4 as a new p-type conducting oxide material,[9] realizing the suitability of a host of previously unknown ABX compounds

A. Mannodi-Kanakkithodi, G. Treich, Dr. T. D. Huan, Dr. R. Ma, M. Tefferi, Dr. Y. Cao, Dr. G. Sotzing, Dr. R. Ramprasad
Institute of Materials Science
University of Connecticut
Storrs, CT 06269, USA
E-mail: rampi.ramprasad@uconn.edu

DOI: 10.1002/adma.201600377

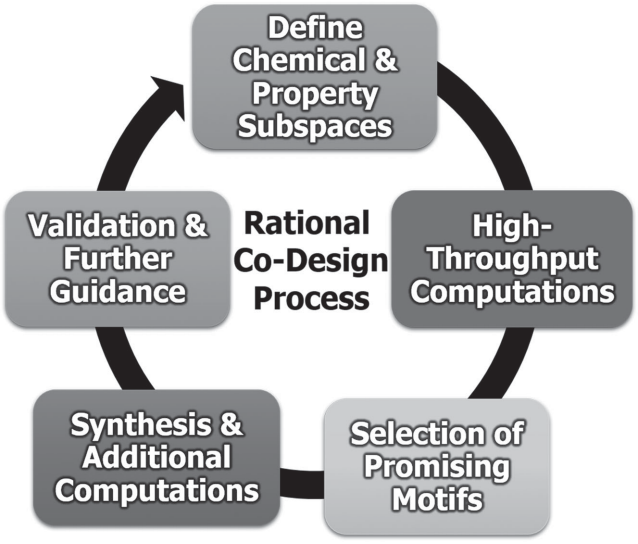

Figure 1. The primary steps involved in a rational co-design approach.

(with 18 electrons) for topological insulators, thermoelectrics, and piezoelectrics,[10] the rational co-design of Co_2-based Heusler compounds for spintronics applications,[11] the creation of advanced catalysts,[12] and the rational design of new organic and organometallic polymer dielectrics,[13–18] the subject of this article. The past successes and future potential of the rational co-design approach have been recognized in terms of initiatives such as the Materials Genome Initiative[19,20] and the Integrated Computational Materials Engineering[21] framework, as well as in terms of the emergence of several useful materials databases.[22–26]

The primary focus of this article is the application of such a rational co-design process for the identification of entirely new polymer dielectrics options for high-energy-density and electrostatic energy-storage applications. The demand for high-energy-density capacitors has gone up in recent years, courtesy of the on-going electrification of land[27,28] and sea[29] transportation, as well as other military and civilian systems.[29,30] Whereas ceramics could conceivably be used as dielectrics in capacitive energy-storage applications, polymers provide a clear advantage as they display "graceful failure" at high electric fields. Since the energy stored in a capacitor is proportional to the dielectric constant and the square of the electric field, dielectric polymers of interest should display a high dielectric constant and high electrical-breakdown field. Low dielectric loss and resistance to high-field degradation of the polymer itself are other important requirements. Biaxially oriented polypropylene (BOPP), with a high breakdown field of about 700 MV m^{-1} and a dielectric constant of about 2.2, is the current state-of-the-art polymer dielectric in high-energy-density (metalized) film capacitors. Attempts to improve upon BOPP have been based on poly(vinylidene fluoride) (PVDF) and its copolymers,[31–37] polymer nanocomposites,[38–40] multilayers,[41–45] and so on. All such potential replacements have suffered from one or another weakness, like high loss or low parallel-plate breakdown field. The history of capacitor materials, including recent advances and persistent challenges underlying new materials development, has been recently reviewed.[46]

Arun Mannodi-Kanakkithodi is currently a Ph.D. student in the Materials Science and Engineering Department at the University of Connecticut. He obtained his Bachelor of Technology (2012) in Metallurgical and Materials Engineering from the Indian Institute of Technology, Roorkee, India. His research is focused on the rational design of new and advanced dielectric polymers using first-principles computations and machine-learning techniques.

Gregory Martin Treich is currently a Ph.D. student in the Polymer Program at the University of Connecticut. He obtained his Bachelor of Science (2013) in Chemistry from Rensselaer Polytechnic Institute. His research interests include dielectric materials for capacitor applications, conductive polymers for wearable electronics, and bio-derived materials.

Rampi Ramprasad is presently a Professor of Materials Science and Engineering at the University of Connecticut. His area of expertise is in the development of quantum mechanics and machine learning based computational tools, and in the application of such methods for the design and discovery of new materials, especially functional, electronic, dielectric and catalytic materials.

Clearly, strategies are needed to identify new promising polymers. Given the vastness of the polymer chemical (and configurational) space, it is safe to assume that significant untapped opportunities exist, and that several new polymer dielectrics are waiting to be discovered. As pointed out above, the availability of modern computational methods, used within a co-design paradigm, provides the opportunity to perform rational and targeted searches for novel dielectrics at reasonable cost;[47] this can extend significantly the reaches of purely empirical Edisonian attempts. Here, we review recent such successful attempts at chemical-space searches that have resulted in the co-design of new organic and organometallic polymer dielectrics appropriate for high-energy-density applications.

2. Organic Polymers as Dielectrics

2.1. Strategy for Initial Rational Computation-Guided Search

With respect to exploring the large polymer chemical spaces for dielectric capabilities, the historical work has generally featured a few limited subclasses/families of polymers. The staggeringly large number of chemical unit possibilities, and the various kinds of possible connectivity sequences of the units giving rise to different polymer repeat units (**Figure 2** provides a flavor), make experimental examination of a substantial number of these systems impractical.

However, a controlled subspace selected out of this vast expanse could be a dataset of polymers that is ripe for high-throughput computational study. This was recently attempted in a study by Sharma et al.,[13] in which the chemical subspace contained the following 7 building blocks: CH_2, CO, NH, C_6H_4, C_4H_2S, CS, and O. Such a set of building blocks was chosen based on their presence in well-known polymer systems, and was deemed to be suitable for performing a controlled computational–experimental study of organic polymers. Several different polymers were generated by linearly connecting randomly chosen blocks out of the set of 7, as shown in **Figure 3**. This led to the possibility of hundreds of different symmetry-unique polymers, assuming that the repeat units were composed of 4 blocks.

First principles computations using density functional theory (DFT)[48,49] were then performed on all such polymers in a high-throughput manner, resulting in the bandgap and the electronic and ionic dielectric constants, denoted by ε_{elec} and ε_{ion}. In the terminology used here, ε_{ion} includes all non-electronic contributions to the dielectric response, including bond stretching and bond (dipole) rotations allowed within a crystalline lattice. The sum of these two quantities, namely, ε_{elec} and ε_{ion}, typically computed within the perturbation formalism of DFT,[50] is the total dielectric constant ε_{tot}, which is relevant for comparison with measurements. For dielectric polymers to maximize the amount of energy stored in a capacitor, the dielectric constant, as well as the dielectric breakdown field, should be high (and the dielectric loss should be low). Given the difficulty in computing the breakdown field (especially the true engineering breakdown field) and the dielectric loss at the low frequencies (kHz) of interest from first principles, the bandgap (known to be correlated with the breakdown field and dielectric loss[46,51]) was used as a proxy instead. Thus, an initial screening criterion of "high dielectric constant" and "large bandgap" was used to down-select suitable polymers.

Using DFT as a tool for estimating the bandgap and dielectric constant, one question arises: how accurate are these estimates with respect to state-of-the-art experimental measurements? In **Figure 4**, we provide a comparison of the DFT

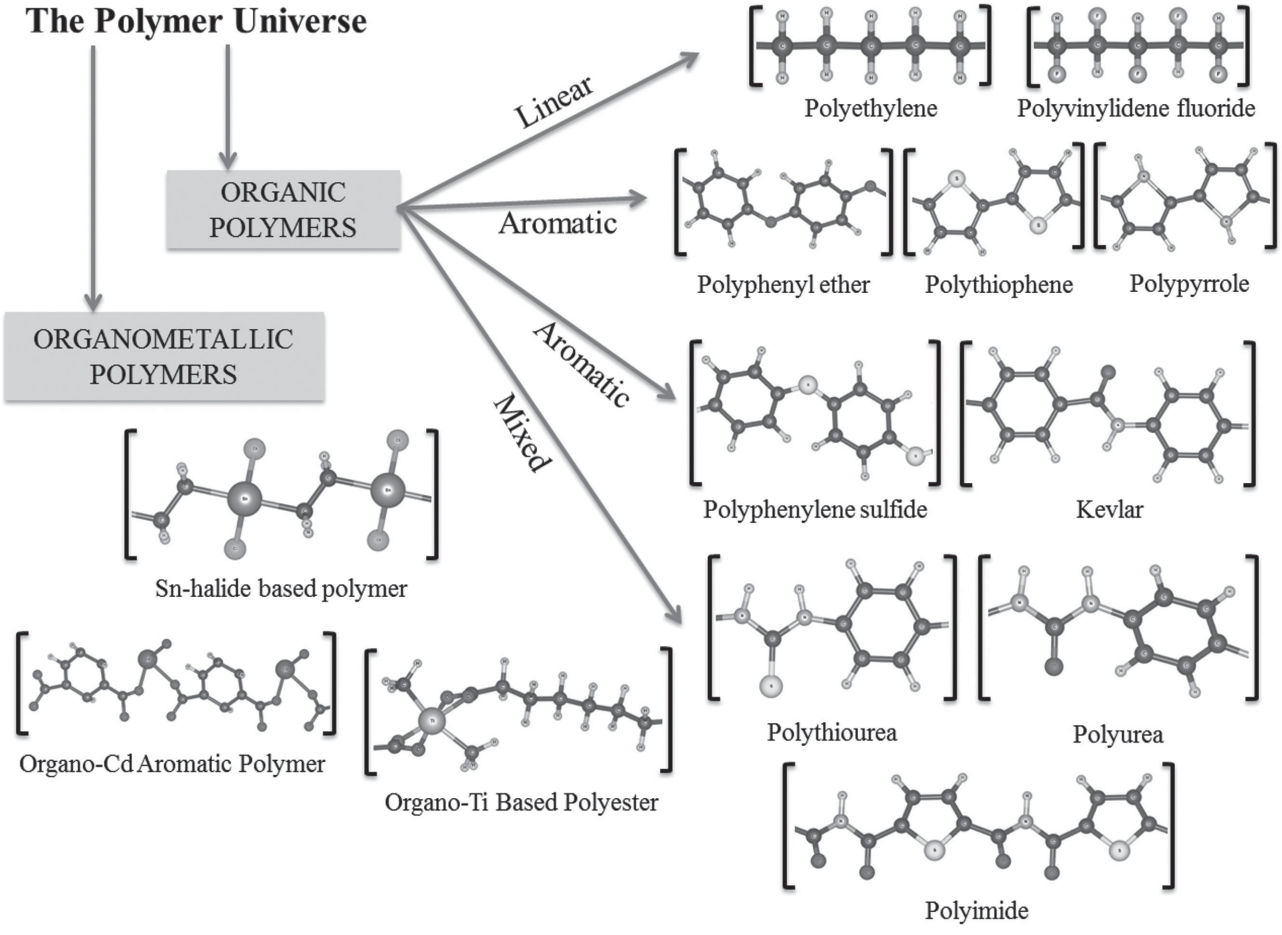

Figure 2. The vast chemical space spanned by a variety of polymer building blocks.

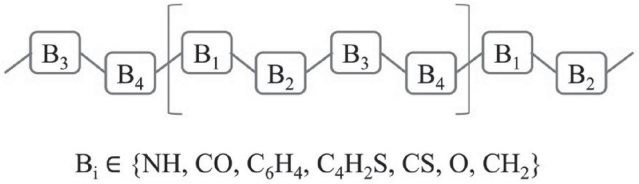

Figure 3. The organic polymer chains selected for high throughput computations.

computed bandgaps and dielectric constants with the corresponding experimental values for a few chosen materials. We show here some inorganic compounds that have been labeled in the plots, a few known polymers—namely polyethylene (PE), polypropylene (PP), polystyrene (PS), poly(ethylene terephthalate) (PET), polyoxymethylene (POM), and poly(ethylene oxide) (PEO)—and, finally, some new polymers that we discuss in detail. It can be seen that the flavors of DFT we use here do indeed help estimate the two properties accurately. The DFT computations are performed on purely crystalline representations of the polymers using fairly reliable (albeit computationally expensive) levels of theory (for instance, using the hybrid Heyd–Scuseria–Ernzerhof (HSE)[52] electronic exchange-correlation functionals for the bandgap as opposed to standard DFT[53]), but the correlation with real-life property measurements is very reasonable. We thus claim that an initial DFT screening step involving the computed bandgap and dielectric constant is a satisfactory approach.

2.2. Initial Computational Guidance

In the investigation by Sharma et al.,[13] hundreds of polymers in their single-chain form, each with a repeat unit made out of 4 building blocks, were considered (see Figure 3 for an illustration). The possible van der Waals and other interactions between chains were ignored at this initial stage for ease and speed of computations. For these single chains, while the bandgap was computed directly using beyond-DFT hybrid functionals as mentioned earlier, the dielectric-constant estimates had to be made by combining DFT with dielectric mixing rules based on effective medium theory.[54] The latter was required as the dielectric constant computed for the single-chain computational setup included a contribution due to an artificial vacuum region that needs to be subtracted out.

With the idea of selecting promising polymer units for high-energy-density applications, the dielectric constants (the electronic component, the ionic component, and the total) were plotted against the electronic bandgaps, as shown in **Figure 5**. Several important insights emerged from this analysis (as well as actual guidance for synthesis). These include:

i) The electronic part of the dielectric constant is inversely correlated to the bandgap (Figure 5a); hence, a large electronic part of the dielectric constant, although desirable (owing to the short timescales of this response) is not safe, as it will lead to poor insulators;
ii) The ionic part of the dielectric constant is immune to the above trend, i.e., it is uncorrelated, or only weakly correlated, to the bandgap (Figure 5b); this contribution to the dielectric constant should thus be exploited;
iii) The best polymers for energy-density applications are those with the best tradeoff between the total dielectric constant and the bandgap. These are indicated by the oval in Figure 5c and include systems predominantly composed of at least one of the polar units, namely –NH–, –CO–, and –O–, and at least one of the aromatic rings, namely $–C_6H_4–$ and $–C_4H_2S–$. –NH–, –CO–, and –O– tend to enhance the ionic part of the dielectric constant, whereas the aromatic groups boost the electronic part.

The last point above immediately provided experimentalists their first vital leads.

2.3. Synthetic Validation of Initial Recommendations

To limit the large amount of data to a sample size that could be analyzed by experimentalists, a threshold for the dielectric

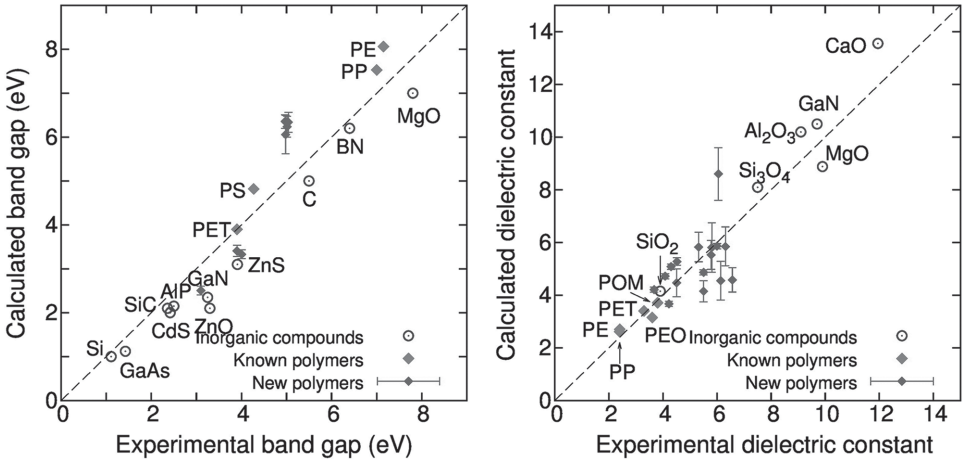

Figure 4. DFT-computed bandgaps and dielectric constants compared with experimental measurements for a few selected inorganic compounds and polymers. The error bars in the calculation results for "new polymers" arise from the different structural configurations of the polymer obtained computationally, as opposed to a single property measurement made on the synthesized polymer.

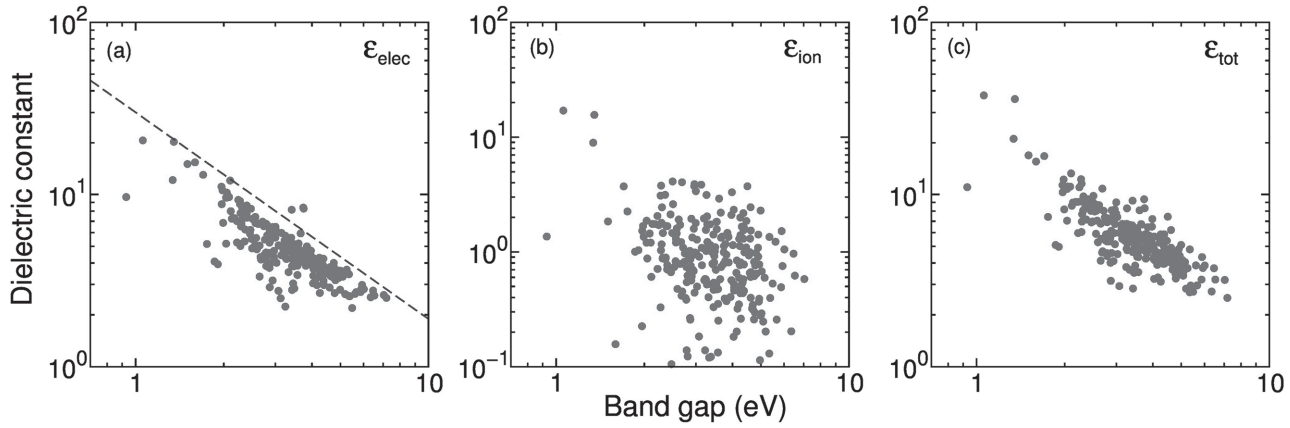

Figure 5. DFT-computed values of: a) electronic, b) ionic, and c) total dielectric constants plotted respectively against the computed bandgap values for the 267 4-block polymers. The dashed line in (a) represents the theoretical limit of the form $\varepsilon_{elec} \leq CE_g^{-1}$ (C is a constant). The small oval in (c) encloses the most promising points with the best tradeoff between the dielectric constant and the bandgap. The data used for this plot were taken from ref. [13].

constant was set at 4 and the lower limit for the bandgap at 3 eV. While a number of polymers (and a number of chemical groups/combinations of groups) were seen to be promising avenues to pursue, three polymers in particular were recommended for synthesis and characterization: –NH–CO–NH–C_6H_4–, –CO–NH–CO–C_6H_4–, and –NH–CS–NH–C_6H_4–. As a synthetic starting point, these three polymers were ideal, as they represented three different polymer classes, namely polyureas, polyimides, and polythioureas, while maintaining the same aromatic unit, C_6H_4.

A number of synthetic routes had to be considered here, as it was not possible to synthesize all the predicted structures by the chemistry known at the time. To fit the criteria of using only 4 structural units, monomers were chosen to obtain repeat-structure units as shown in **Figure 6**. Polymerizations to create all three down-selected candidates proceeded in a stepwise mechanism leading to condensation polymers, which limited the amount of byproducts and side reactions that would ultimately become impurities and interfere with dielectric spectroscopy measurements.

Traditional polymer characterization techniques were employed to study the synthesized polymers. Fourier transform infrared (FTIR) spectroscopy was used to confirm the chemical structure, X-ray diffraction (XRD) to determine the crystalline structure, and UV–vis spectroscopy to estimate the bandgap. Furthermore, time-domain dielectric spectroscopy (TDDS) was employed to study the dependence of the dielectric properties on the frequency. Meanwhile, the crystal structures, morphologies, and relevant properties were studied in greater detail and with more accuracy using computations. The isolated chain model was discarded in favor of polymer chains stacked next to each other in a unit cell, and the respective ground-state 3D structural arrangements of the polymers were determined using two complementary and different approaches: a structure-prediction algorithm (USPEX) using the DFT energies,[55,56] and a melt-and-quench approach using empirical force fields, based on molecular dynamics. Once the most stable crystal structures were obtained, the bandgap and dielectric constant were calculated using DFT, specifically using the HSE functional[52] for the bandgap and density functional perturbation theory (DFPT)[50] for the calculations of the dielectric constant. While the dielectric constants were found to range from 4 to 6, which is double that of PE or PP, the bandgaps were seen to be greater than 3 eV.

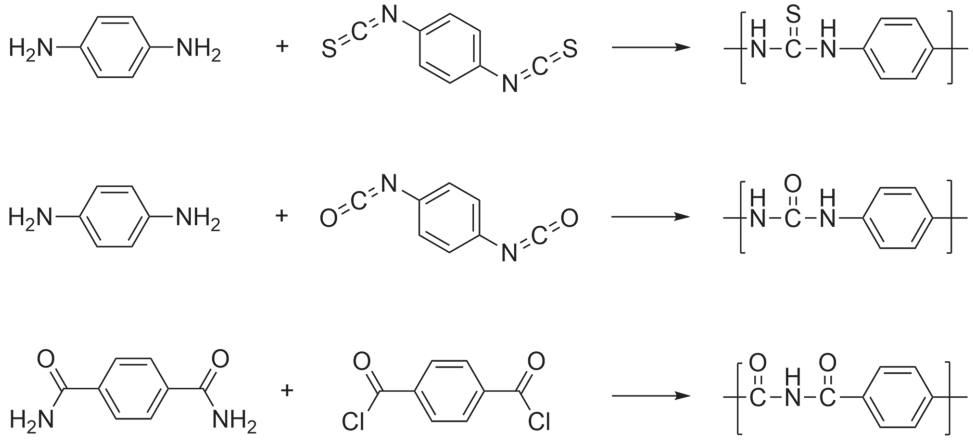

Figure 6. Synthetic scheme for the three down-selected organic polymers in ref. [13].

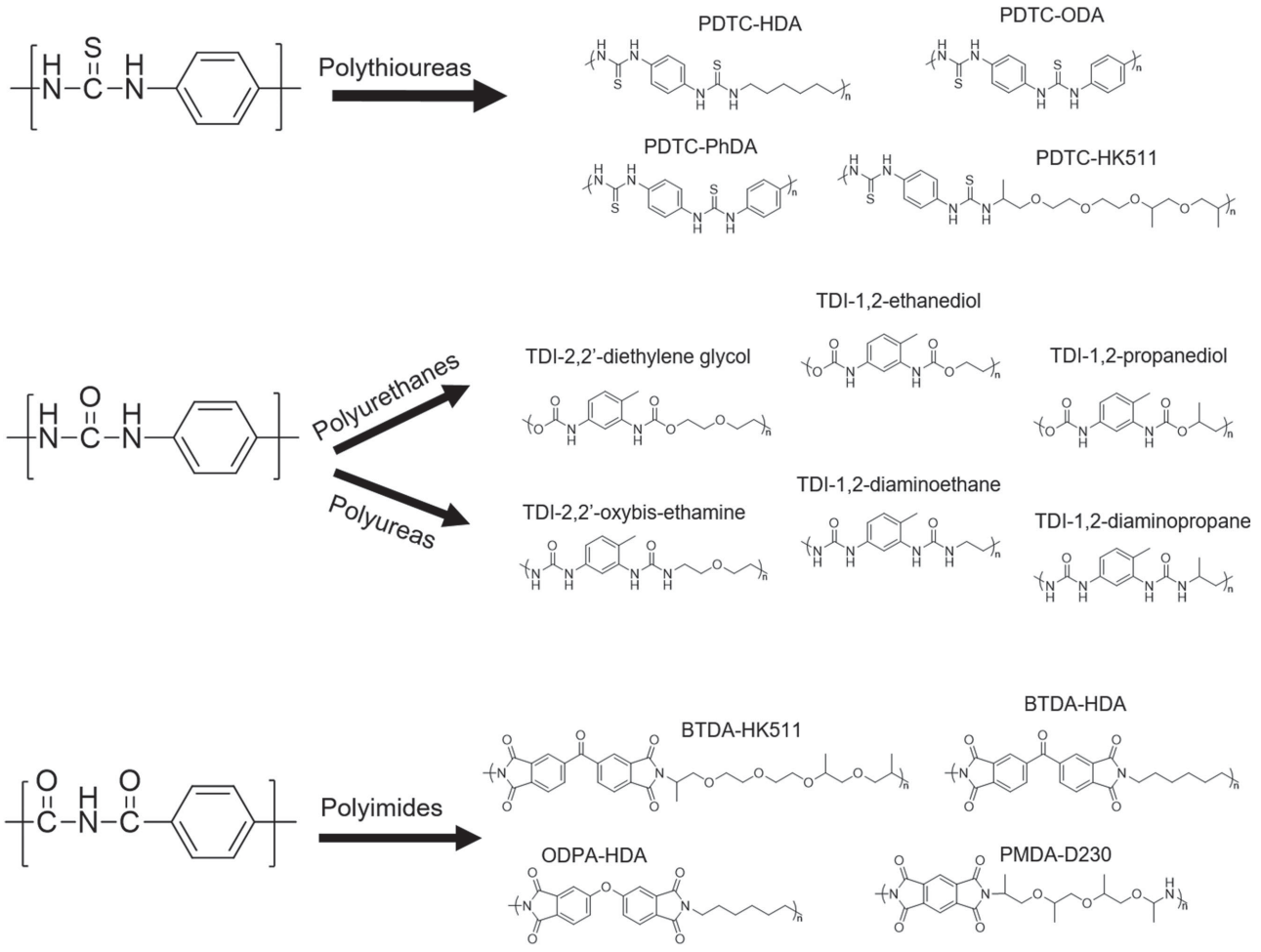

Figure 7. Extensions to new polythioureas, polyureas, polyurethanes, and polyimides.

All computed values were close to experimentally measured values. Because of the consistency of the DFT results with the melt-and-quench approach, the DFT-predicted ground-state structures are expected to be stable at elevated temperatures as well, and thus, these computed property values are expected to stand at higher temperatures. Despite the fact that all predictions are made for purely crystalline structures and the synthesized polymers are largely semicrystalline or amorphous, the measured dielectric-constant ranges matched up very well with predictions for the three polymers. Thus, a "computations → experiments → computations" synergistic loop was successfully pursued in the design of new organic polymer dielectrics.

The success of the initial mating between DFT calculations and synthetic efforts for dielectric studies gave way to other possible systems to be developed using the same initial computational data. The synthetic efforts branched into three different studies, each involving a different polymer class to further understand the theoretical and experimental properties of proposed organic dielectrics. As shown in **Figure 7**, the three polymers studied at first and discussed above gave way to the study of a number of: i) polythioureas, ii) polyureas, and urethanes, and iii) polyimides.

2.4. Reduction to Practice: Polythioureas

The first polythiourea synthesized, –NH–CS–NH–C_6H_4–, provided a simple structure for calculations and synthesis; however, the actual synthesized material proved to be insoluble and was seen to melt at or above its degradation temperature, and was therefore not processable into thin films. Ma et al.[57] studied polythioureas with longer and more flexible chains with the idea of improving the processability. By keeping one monomer constant, para-phenylene diisothiocyanate (PDTC), and by varying the diamines between different aromatic, aliphatic, and polyether monomers, structure–property relationships were derived for the dielectric constant of this family of polythioureas. Five different diamines were chosen: 4,4′-oxydianiline (ODA), bis(4-aminophenyl)methane (MDA), 1,4-diaminobenzene (PhDA), hexane-1,6-diamine (HDA), and jeffamine HK511. Further, a thiophosgene reaction was employed to mimic an industrial-scale reaction for the polymerization of a related thiourea compound reported by Wu et al.[58] The six polymers thus studied are listed in **Table 1**, and the structures of some of them are shown in Figure 7.

Extensive polymer characterization was carried out on these polythioureas; this included obtaining their respective FTIR,

Table 1. Experimental and computational (shown in brackets) dielectric data for polythioureas. The measured ε_{tot} and tanδ correspond to room temperature (r.t.) and a frequency of 1 kHz; ε_{elec} is reported as the squared value of the measured refractive index.

Polymer	ε_{elec}	ε_{tot}	tanδ	E_g [eV]
PDTC-ODA	3.20 (3.86)	4.52 (5.42)	0.0233	3.22 (3.27)
PDTC-MDA	3.28 (3.69)	4.08 (4.59)	0.0348	3.16 (3.41)
PDTC-PhDA	N/A	4.89	0.0144	3.07
PDTC-HDA	2.92 (3.29)	3.67 (4.01)	0.0267	3.53 (3.75)
PDTC-HK511	2.69	6.09	0.0115	3.51
Thiophosgene-MDA	3.03	3.84	0.0226	3.3

XRD, and solution NMR spectra to determine the structure. Further computations were performed on these specific polythioureas in order to obtain more-accurate property estimates, and were compared with experimental results. The low-energy polymer configurations obtained as before[13,55,56] were subjected to electronic- and dielectric-property computations.

The measured ε_{tot}, E_g, and dielectric loss for these polythioureas are shown in Table 1; the corresponding computed values are shown in brackets for comparison. To determine ε_{elec} experimentally, the refractive index was measured by ellipsometry; the square of the refractive index is equivalent to ε_{elec}, and these values have also been reported in Table 1.[59] The experimentally determined ε_{elec} and ε_{tot} are comparable to but lower than the calculated DFT values. These discrepancies are probably due to calculations being done solely on the crystalline polymer state, whereas experimental measurements are averages over the crystalline and amorphous regions. This is confirmed by comparison of calculated and experimental IR and XRD spectra of both fiber precipitates and solution-cast films. While the IR spectra for the synthesized samples and the predicted structures are in close agreement, the XRD patterns of the synthesized fibers are in closer agreement with the XRD spectra of the predicted structures, indicating the larger crystalline content of these samples, whereas the films are generally amorphous. TDDS results for one of these polythioureas, namely PDTC-HDA (the polymer made from 1,4-diisothiocyanatobenzene and hexane-1,6-diamine), are shown in **Figure 8**a (this polymer is shown at the top of Figure 7). While the dielectric constant is shown to increase with operational temperature due to the chains becoming more mobile and thus enhancing dipole alignment, this effect is diminished at high frequencies, as the dipoles are unable to align as quickly.

While the bandgap provides a good theoretical substitute for the dielectric breakdown-field strength since a higher bandgap would imply a higher threshold for impact ionization, access to the breakdown field is possible through either direct breakdown measurements or electric displacement–electric field (D–E) loop measurements. The latter measurements also provide a pathway to assess linearity and energy recovery, and to obtain energy-density estimates. Such D–E measurements were done for PDTC-HDA, and this is shown in Figure 8b. The recoverable energy density as a function of the applied electric field is shown in Figure 8c. The ability to operate at high electric fields would lead to a significant increase in energy density. For PDTC-HDA, a high energy density of 9.3 J cm^{-3} was achieved at a maximum applied field of 685 MV m^{-1}, which is a substantial energy-density improvement over BOPP (almost double its value). The maximum energy density is expected to further improve with better processing conditions to remove contaminants such as dust impurities and residual solvent, as this will lead to higher values of the breakdown field. An important point worth noting is that, although the initial computational screening was based just on the dielectric constant and bandgap, the directions identified, in terms of materials subclasses to pursue, have led to polymers with acceptable dielectric loss and high breakdown field (and hence, energy density).

2.5. Polyureas and Polyurethanes

After having a successful correspondence between expected values from DFT and experimental results for the 4-block polyurea originally recommended, namely, –NH–CO–NH–C_6H_4– (with ε_{tot} greater than 5 and E_g above 3 eV), synthetic efforts returned to the urea structure. To increase experimental variation in the tested systems, two sets of nearly identical polymers were studied: one comprising polyureas and the other a related class, polyurethanes.[15] Polyurethanes were attractive for this

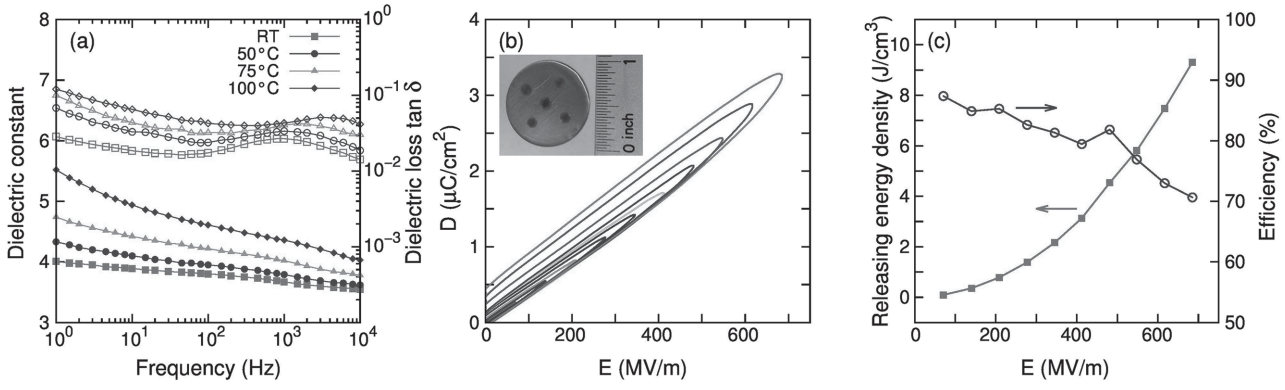

Figure 8. a) Dielectric constant (bottom curves) and dielectric loss tanδ (top curves) measured at room temperature (RT), 50 °C, 75 °C, and 100 °C, b) D–E loops, and c) the releasing energy density and efficiency of PDTC-HDA. A film of PDTC-HDA is also shown in (b) as an inset. Figure 8 is plotted from the data reported in ref. [57].

Table 2. Measured dielectric constant and loss values for the polyureas and polyurethanes.

Polymer	ε_{1kHz}	$\tan\delta_{1kHz}$ [%]
1A	5.18	0.758
2A	4.29	0.889
3A	3.47	1.73
4A	2.08	3.12
5A	6.19	4.29
1B	6.35	1.26
2B	6.74	1.54
3B	5.81	1.39
4B	4.09	1.56
5B	10.5	1.88

comparison as the reaction is very similar, substituting out diamines for dialcohols and adding in a small amount of dibutyltin dilaurate catalyst. All other reaction conditions were held the same in both cases to give comparable results.

In this case, 5 diamines and their respective diols (which act as polar segments) were polymerized along with toluene diisocyanates (TDI); select polyureas and polyurethanes are shown in Figure 7. The polymers were purified and dried before being characterized structurally, thermally, and electronically by gel-permeation chromatography (GPC), NMR, thermogravimetric analysis (TGA), differential scanning calorimetry (DSC), and TDDS; the results for a series of polyureas (labeled 1A–5A; here, different alkyl and aromatic groups are flanked by –NH–CO–NH– units) and the corresponding polyureathanes (labeled 1B–5B; the same groups are flanked by –NH–CO–O– units) are tabulated in **Table 2**.

In general, the polyurethanes showed a higher ε_{tot} than their corresponding polyurea cousins, which can be explained by the higher electronegativity of the urethane group compared to the urea group. Also following the same electronegativity argument is the fact that more carbon atoms in the backbone decreased the value of ε_{tot} across the board, as carbon has a diluting effect on the urea and urethane linkages as shown in previous studies.[60,61] The increase in ε_{tot} seen in polymers 5A and 5B shows the beneficial effect of adding ethers into the backbone of polymers on dielectric constant, and agrees with previously reported values for polyether urethanes.[62] In summary, this study confirmed that the best ways to increase the dielectric constant in aromatic polyurea and polyurethanes involves maximizing polarizability through electronegative atoms such as oxygen, and decreasing carbon in the backbone to maximize the contribution from the functional groups. Further extensive studies and optimization are required to realize practically useful polyureas and polyurethanes. Such work is in progress.

2.6. Polyimides

Polyimides are attractive for dielectric applications due to their high thermal stability, which allows them to have a higher operational temperature than traditional polymers such as BOPP. Inspired by the identification of polyimides as an attractive subclass in the initial computation-based screening, Ma et al.[14] synthesized ten polyimides by choosing four different rigid aromatic dianhydrides, namely pyromellitic dianhydride (PMDA), 3,3′,4,4′-benzophenone tetracarboxylic dianhydride (BTDA), 4,4′-oxydiphthalic anhydride (OPDA), and 4,4'-hexafluoroisopropylidene diphthalic anhydride (6FDA), along with two flexible diamines with aliphatic chains of different lengths, propane-1,3-diamine (DAP) and hexane-1,6-diamine (HDA). Also chosen were two different ethers containing jeffamines (D230 and HK511), based on previous positive results. In this fashion, 10 polyimides were studied, some of which are shown in Figure 7. The measured bandgap, dielectric constant, and dielectric loss of these polymers are shown in **Figure 9**.

The dipolar polarizability of the imide functional group leads to all the polyimides having higher dielectric constants than BOPP. It can be seen from Figure 9b that the polyimide BTDA-HK511 showed the highest ε_{tot} of 7.8, which is in large part due to the orientational polarization imparted by the polyether section. BTDA-HK511 was also seen to have one of the lowest dielectric loss values of all the polyimides shown in Figure 9c, around 0.5%, while being able to operate at temperatures up to 75 °C. Large-scale free-standing films could be made out of this polymer, as shown in **Figure 10**a. Results of TDDS measurements performed at increasing temperatures on BTDA-HK511 are plotted in Figure 10b, and a Weibull plot of the breakdown

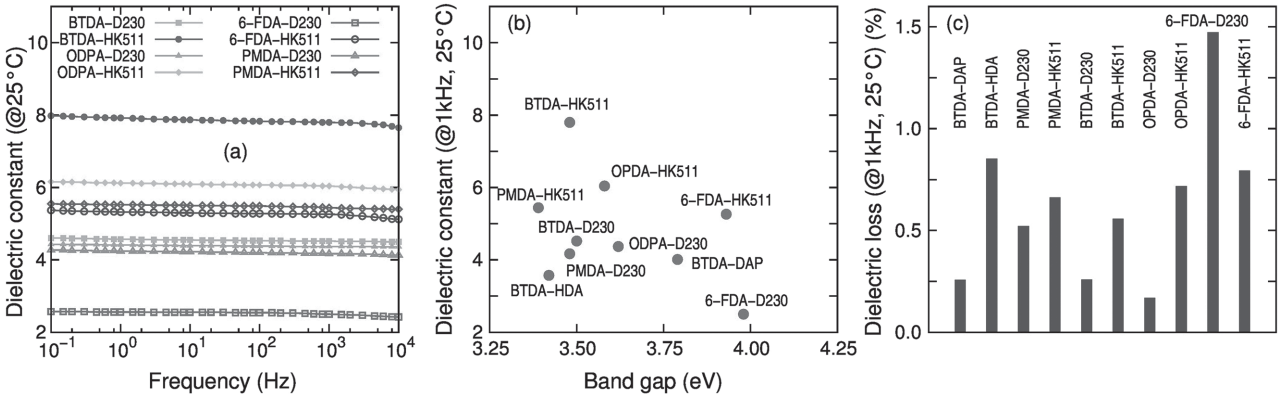

Figure 9. a) The dielectric constant measured for all the polyimides at room temperature (25 °C) given as function of frequency. b) Dielectric constants measured at 1 kHz plotted against the bandgaps. c) Dielectric losses measured at 1 kHz. Figure 9 is plotted from the data reported in ref. [14].

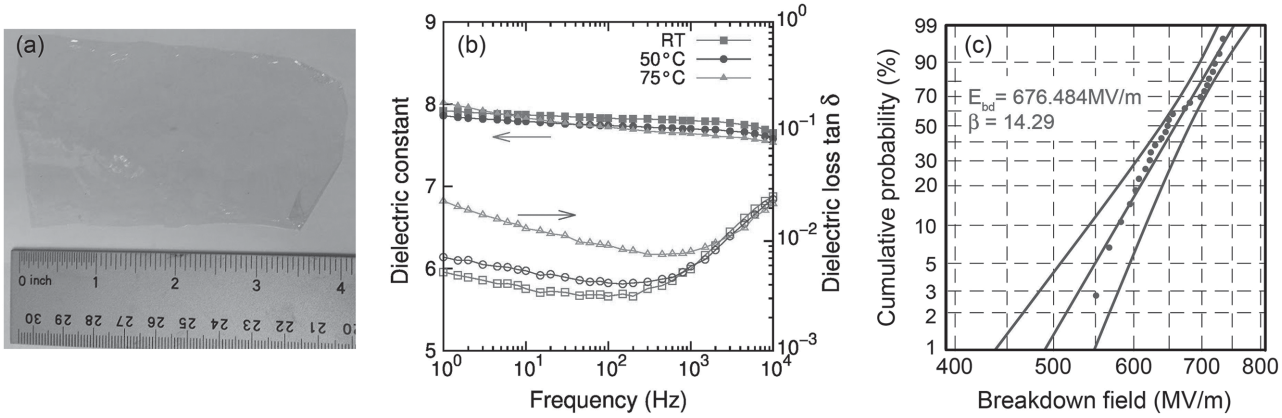

Figure 10. a) A solvent-cast free-standing film of BTDA-HK511 with a thickness of 12 μm. b) The dielectric constant and loss at room temperature (RT), 50 °C, and 75 °C. c) Weibull plot of dielectric breakdown, with the characteristic breakdown field and the slope parameter indicated. Figure 10 is plotted from the data reported in ref. [14].

measurements for BTDA-HK511 is shown in Figure 10c. It was concluded that, while the dielectric constant decreases with frequency due to slower orientation of the dipoles with alternating electric fields, dielectric loss increases because of chain relaxations. The Weibull analysis was used to determine a characteristic breakdown field of 676 MV m^{-1}, as shown in Figure 10c. For a straight comparison, the same exercise was performed for the polyimide that formed the best films, namely, BTDA-HDA, which displayed the highest breakdown field (among all polyimides considered here) of 812 MV m^{-1}, although with a modest dielectric constant of less than 4. The respectable breakdown field of BTDA-HK511 along with its high dielectric constant of 7.8 corresponds to a possible energy density of 15.77 J cm^{-3}. This is nearly three times that of BOPP. The co-design approach has thus led to a number of polymer dielectrics that could potentially surpass BOPP in actual applications.

3. Organometallic Polymer Dielectrics

3.1. Rationale for Exploring Chemical Spaces beyond Purely Organic Systems

Organometallic polymers, i.e., those containing metal atoms covalently bonded within their backbones, are outside the chemical subspace of the organic polymers. The development of such polymers for energy storage[16–18] was guided by several rational considerations, aiming specifically at boosting the ionic dielectric constant ε_{ion}, given a certain high bandgap (the importance of the ionic contribution was already pointed out in the context of organic polymers; see for instance Figure 5, and the insights that emerged from its analysis). Two of the primary considerations in favor of incorporating non-carbon species (e.g., metals or even semiconducting systems in their bulk forms) in polymers are as follows. First, metal-containing bonds may be highly polar, depending on the nature of the metal. Second, the lattice vibrations involving these bonds are generally low in frequency. Both of these factors are crucial for an improvement of ε_{ion} at the low-frequency limit,[46] while, according to Huan et al.,[63] the electronic dielectric constant ε_{elec} of polymers in this class is also confined by the same theoretical limit shown in Figure 5b and discussed in Section 2.2. Once again, it should be remembered that ε_{ion} includes all non-electronic contributions to the dielectric response, including bond stretching and bond (dipole) rotations allowed within a crystalline lattice.

The expected improvement of ε_{ion} was soon confirmed in a report on high-throughput screening based on DFT computations.[64] By establishing a large number of single polymeric chains containing different blocks based on C, Si, Ge, and Sn, the bandgap and the dielectric constants were computed. A summary of the resulting data is shown in **Figure 11**a; an overall inverse relationship can be seen between the two properties, similar to the trends observed in Figure 5. This places a bound on one property when increasing the other; the polymer chains containing polar units such as SnF_2, $SnCl_2$, GeF_2, and $GeCl_2$ dominate the upper-left portion of the plot, where dielectric constants are as high as 30, while the bandgaps are

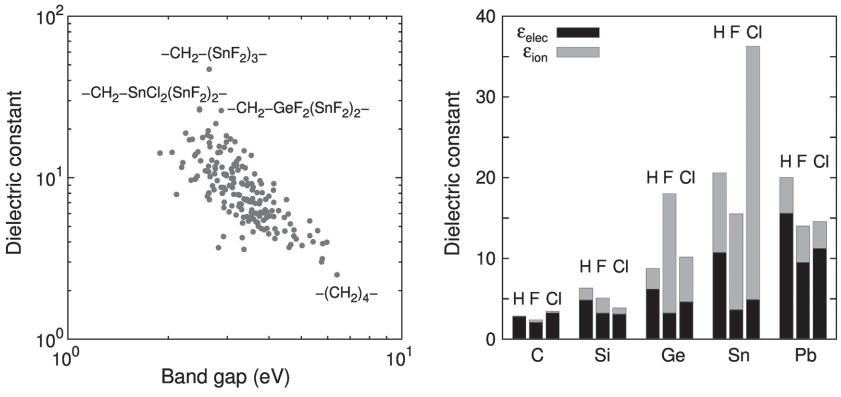

Figure 11. Left) Computed dielectric constants shown vs bandgaps of single-chain polymers formed from C, Si, Ge, and Sn based units,[64] and (right) the electronic and ionic dielectric constants of compounds of group-14 elements.[65]

around 3–4 eV. Most importantly, this study also revealed key correlations between ε_{ion} and the dipole moments and rotational barriers to the dipoles from adjoining groups.

This interesting observation suggests a systematic examination of group-14 elements, i.e., C, Si, Ge, Sn, and Pb; these systems, in their elemental bulk forms, range from insulators to semiconductors to metals. DFT computations were performed on the hydrides, fluorides, and chlorides based on these elements;[65] the computed ε_{elec} and ε_{ion} of these binaries are shown in Figure 11b. Compared to C- and Si-based compounds, the ionic dielectric constants of the Ge-, Pb-, and especially, Sn-based materials, are extremely high. These initial studies provided the rationale for the recommendation that incorporation of Sn into typical organic polymer backbones, potentially bonded with highly electronegative atoms such as F, Cl, or O, may be beneficial.

3.2. Poly(dimethyltin glutarate) and Poly(dimethyltin esters)

Based on the computational guidance, Sn was selected for developing new organometallic polymers.[16,17] An organotin functional group, Sn ester, was identified as the starting point due to the large electronegativity difference between Sn and oxygen (O). The actual synthesis was performed using dimethyltin dichloride and glutaric acid, resulting in poly(dimethyltin glutarate), or p(DMTGlu), a new polymer in which the repeat unit contains a dimethyltin group flanked on either side by a carboxylate group, with a linear chain of 3 methylene (CH_2) units acting as the linker.[16] The synthesis scheme, as shown in **Figure 12**, was altered from that proposed by Carraher Jr. and Roner[66] by using tetrahydrofuran (THF) instead of hexane. This change allows for a traditional condensation polymerization instead of an interfacial polymerization, while the added polarity of THF helped to solubilize the growing chain and to produce higher-molecular-weight polymers. The resulting polymer, p(DMTGlu), is thermally stable at temperatures up to 235 °C while showing a high dielectric constant larger than 6. In terms of high-*T* capability and dielectric constant, p(DMTGlu) is superior to most currently used organic dielectric polymers, e.g., BOPP, which has a dielectric constant of 2.2 and works at temperatures below 105 °C.[67] Although the thermal stability of p(DMTGlu) is still below that of some recently developed polyimides,[14,68] there is a clear indication that tin-based organometallic polymers can combine both high-*T* capability and a high dielectric constant. Given the success in developing p(DMTGlu), a complete series of related poly(dimethyltin esters) has then been synthesized.[17] All the polymers in this family are based on the dimethyltin-ester group, differing from p(DMTGlu) and from each other by the number of methylene units in the linker, which ranges from 0 to 11. The whole family of polymers has since been processed and characterized.[16,17] As some of them

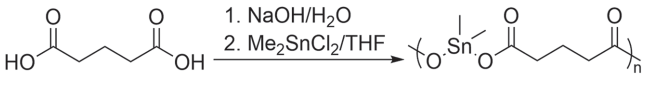

Figure 12. Synthetic route to poly(dimethyltin glutarate).The repeat unit of the resulting polymer contains a dimethyltin group and a linker of 3 methylene (CH_2) groups.[16]

are not soluble, desired measurements had to be performed either on cast films or on pellets made of these polymers.

In parallel with the experimental effort, detailed first-principles calculations were performed for this family of organotin polymers.[16,17] In brief, the structures of these polymers were determined by the minima-hopping structure-prediction method,[69,70] starting from the polymeric chains of the predetermined repeat units. Because Sn can adopt a variety of coordination environments, the geometry of the Sn-containing units is not well defined. Thus, the structure-prediction step had to be done without constraints. Further calculations were then performed on the most stable structures at suitable levels of DFT, determining the dielectric constant with DFPT[50] and bandgap using either the Perdew–Burke–Ernzerhof (PBE)[71] or HSE electronic exchange-correlation functional.[52] Calculation at the PBE level of DFT is fast, but the result is typically underestimated by 30% or more,[53] while HSE offers more reliable results at sufficiently higher computational cost. For the purpose of methodology validation, IR spectra and XRD patterns were obtained from simulations as well.

In the predicted structures of the poly(dimethyltin esters), all the Sn atoms are six-fold coordinated. The Sn–O bonds, on the other hand, can link different polymeric chains in various ways.[16,17] This feature distinguishes these organometallic polymers from their organic counterparts, in which the polymeric chains are essentially isolated. Depending on the arrangement of the Sn–O bonds, three basic motifs, namely intrachain (α), interchain (β), and hybrid (γ, which combines some features of α and β), were identified. These motifs, which are shown in **Figure 13**, can exist simultaneously in the synthesized samples because they only differ from each other by a few meV per atom. Of these, the intrachain and interchain motifs have been documented in the literature for some organotin materials.[72] The existence of these motifs in the synthesized samples was confirmed by comparison of the computed and measured IR spectra and XRD patterns.[16,17]

The dielectric constant and the bandgap of the poly(dimethyltin esters) depend on the length of the linker (or the number of the methylene units) in certain ways. **Figure 14** compiles the computed and measured data for these essential quantities, revealing that, in general, the dielectric constant is decreased and the bandgap is increased when the linker is longer. There are, however, some "optimal" lengths of the linker (4–7 methylene units) at which both the bandgap and the dielectric constants are high. For the particular case of poly(dimethyltin suberate) (or pDMTSub, the poly(dimethyltin ester) that contains a linker of 6 methylene groups), the dielectric constant can be as high as 7, and, at the same time, the bandgap reaches a value of nearly 7 eV. The refractive index, the square of which is the electronic dielectric constant ε_{elec}, was measured for some cases, leading to a good agreement with the calculated data.[16,17]

To access the dielectric breakdown strength of the poly(dimethyltin esters), their charge–discharge behavior was determined through the *D*–*E* hysteresis loop. Because these polymers form large crystalline phases upon drying, whose size depends on the length of the methylene linker, they were blended with a second homopolymer, which is poly(dimethyltin 3,3,-dimethylglutarate), or pDMTDMG, to produce an amorphous morphology. Films can then be cast for the desired

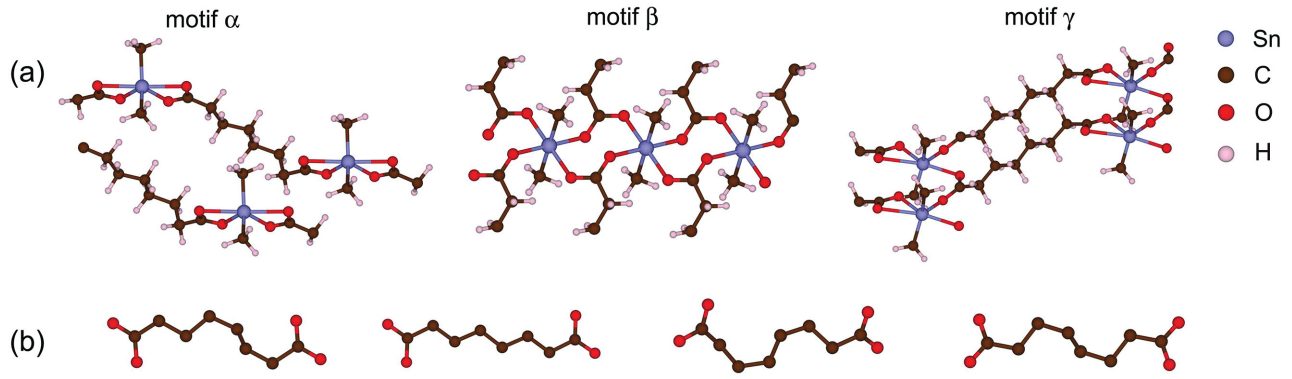

Figure 13. a) Three basic structural motifs (α, β, and γ) computationally predicted for poly(dimethyltin esters). b) Some folding patterns of the methylene linker. Reproduced with permission.[17] Copyright 2015, American Chemical Society.

measurements. The hysteresis loops obtained for a blend consisting of a 20/80 (wt/wt) pDMTDMG/pDMTSub are shown in Figure 14c, while those of the pDMTDMG/pDMTGlu were reported by Baldwin et al.[16] The measured data suggests that pDMTGlu and pDMTSub are linear dielectrics with breakdown strengths of roughly 400 MV m^{-1} and 300 MV m^{-1}, respectively, leading to an energy density of roughly 4 J cm^{-3}. Although this parameter is still below that of BOPP (5 J cm^{-3}), the new chemical subspace of the organometallic polymers looks promising, given that we are at the very initial stages of optimization of this entirely new polymer subclass. More importantly, the pathway leading to the development of these organotin polymers can be used for further exploration into this subspace (and for expanding the search space beyond just organotin polymers, as briefly discussed later).

3.3. Effects of Aromatic and Chiral Groups on the Dielectric Properties of Poly(dimethyltin esters)

While the initial rationale leading to the development of poly(dimethyltin esters) focused on tin-containing groups, the linker does play an important role. With the linker containing a given number of methylene units only, the effect of the linker length on the dielectric constant and the bandgap is shown in Figure 14. If other building blocks like aromatic and chiral groups are introduced in the linker (see **Figure 15**), the dielectric properties can be further manipulated.

In recent work on these lines, Baldwin et al.[18] concluded that the size and the electron density/polarity of the aromatic rings have certain effects on the dielectric constant. As the size of the ring is increased, the resulting dielectric constant would be lower. The nature of the aromatic rings is also relevant. In particular, polymers containing (electron-neutral) benzene rings would have higher average dielectric constants compared to those having (electron-donating) thiophene rings or (electron-withdrawing) pyridine rings. Chiral groups can be used to control the crystallinity of the polymers, which, in turn, affects the averaged dielectric constant. It is clear that substantial room is available for optimizing the dielectric properties of the poly(dimethyltin esters).

3.4. Prospects of Going Beyond Organotin Polymers

While Sn is clearly an appealing ingredient for the development of organometallic polymers for high-energy-density applications,

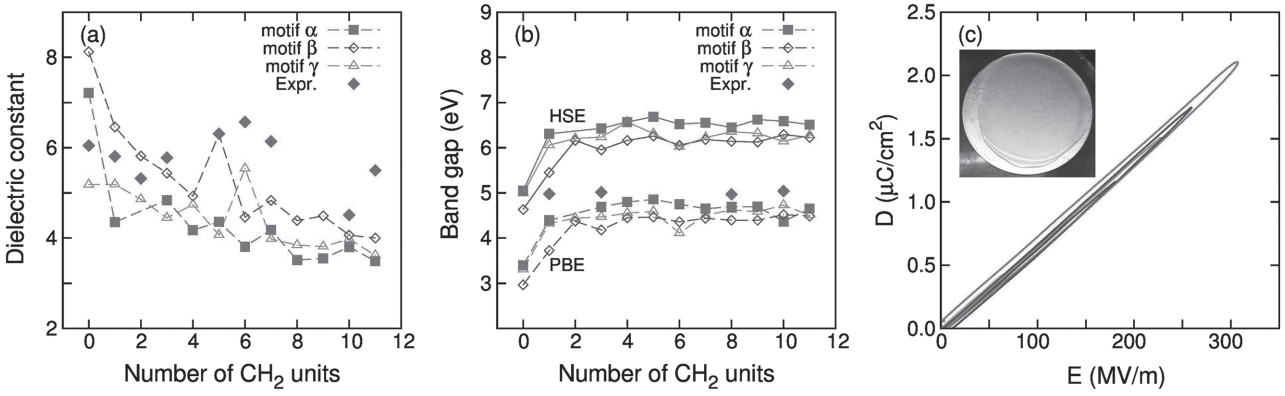

Figure 14. Computed and measured data for: a) dielectric constants and b) bandgaps (calculated at PBE and HSE levels of theory) of the poly(dimethyltin esters) in different motifs (α, β, and γ) with different linker lengths, ranging from 0 to 11 methylene (CH_2) units. In (c), the D–E loops measured for the 20/80 (wt/wt) blend of pDMTSub/pDMTDMG are shown together with a film cast for this polymer in the inset. Figure 14 is plotted from the data reported in ref. [17].

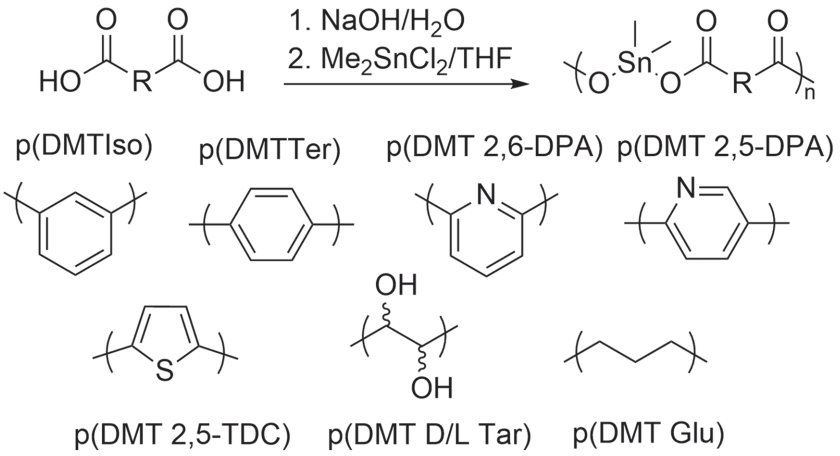

Figure 15. Synthetic scheme of poly(dimethyltin esters) with aromatic (pyridine, benzene, and thiophene) and chiral (tartaric acid) groups.[18]

it is natural to raise the question as to whether other metals can play a similar role. In an extensive recent computational study, ten metals were examined, leading to a dataset of more than one thousand organic and organometallic materials[63] (a detailed description of the dataset is given in ref. [63]). This dataset is summarized in **Figure 16**, demonstrating the clear benefit of metal-atom incorporation in the polymer backbone. As can be seen, the organic and organometallic classes of materials are clearly partitioned into two distinct groups. For a given bandgap, the accessible dielectric constant of the organometallic materials is, in general, superior to that of the organic materials (within the scope of the adopted initial screening criteria). Although in practice, synthesis and processability challenges are bound to arise with these newer subclasses of polymers, the guidance provided by Figure 16 is unmistakable. Rationally selecting and incorporating metals in polymer backbones is surely worthy of future exploration, and will take us to a domain of the chemical space previously unexplored within the context of polymer dielectrics for high-energy-density (or electronics) applications.

4. Outlook

It has been argued here that modern computational methods used synergistically with synthesis, processing, and characterization efforts, and with appropriately defined initial screening criteria, provide the opportunity to systematically and effectively search for novel, previously unknown (or known, but never considered) application-specific materials. This co-design paradigm may be more powerful, more efficient, more cost-effective, more insightful, and more rewarding than just computational or just experimental approaches, and can extend significantly the reaches of purely Edisonian attempts to materials discovery. Here, we have used the example of polymer dielectrics for high-energy-density applications as an example to illustrate how one may harness the co-design concept to go beyond "standard" materials (such as biaxially oriented polypropylene). Recent successes are highlighted, which range from the identification of several new organic polymer dielectrics within known generic polymer subclasses (e.g., polyurea, polythiourea, polyimide), and the recognition of the untapped potential inherent in entirely new and unanticipated chemical subspaces offered by organometallic polymers.

Nevertheless, it must be emphasized that the road from scientific discovery to practical applications is arduous, and punctuated with numerous barriers. For the example of polymer dielectrics for high-energy-density applications discussed here, several fundamental and practical hierarchical considerations including dielectric, electronic, morphological, processing, cost, reliability, and electrical characteristics, need to be addressed and confronted before next-generation materials can be ushered into actual technologies. These issues, challenges, and opportunities were recently reviewed in detail.[46]

Here, we have mainly focused on the aspect of materials discovery. Even within this restricted context, challenges remain. The initial screening criteria adopted here were based on just the dielectric constant and the bandgap. It is true that these seemingly simplistic criteria did lead us to chemical spaces that one is unlikely to have "stumbled upon" serendipitously, and to polymers that, in the end, display an attractive dielectric response. Still, other materials attributes, including dielectric

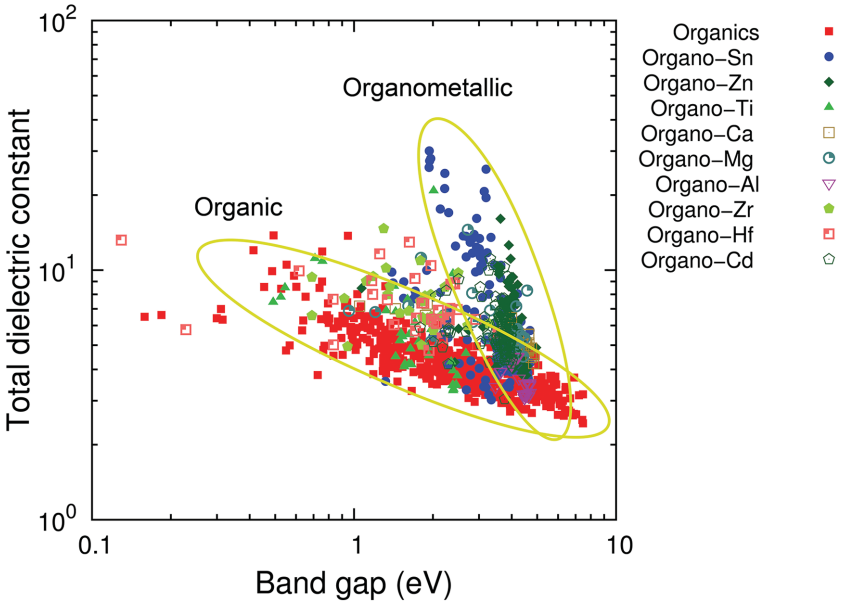

Figure 16. Computed dielectric constant of more than one thousand organic and organometallic materials, shown again their computed bandgap. Two ovals are used to indicate the different regions occupied by the organic and organometallic materials. The data used in this figure were taken from ref. [63].

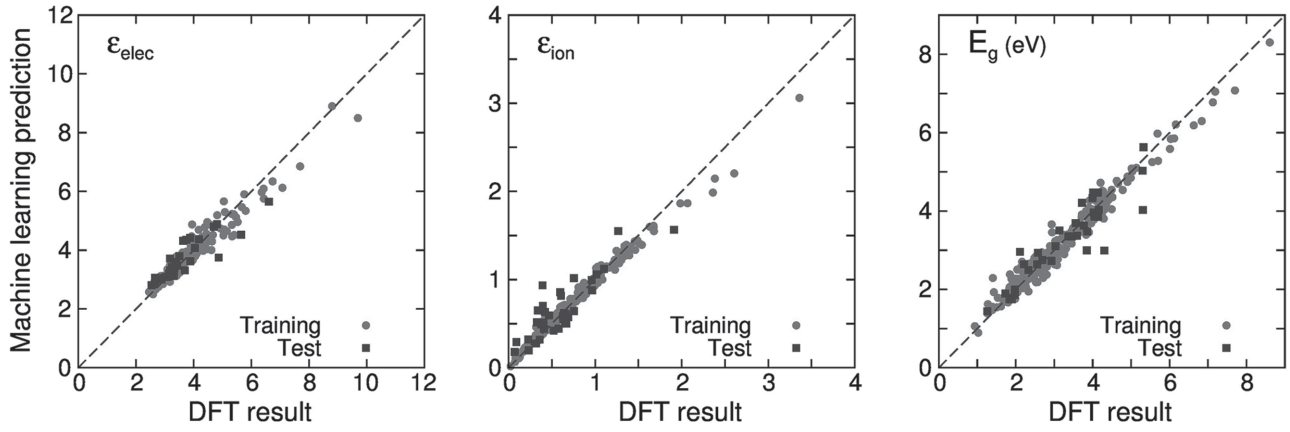

Figure 17. Comparison of machine-learning model predictions with actual DFT results for the organic polymer dataset shown in Figure 5, for three properties: ε_{elec}, ε_{ion}, and E_{gap}. A subset of the total dataset called the Training set (shown in red) was used for training the model, and the remining points in the dataset, called the Test set (shown in blue), were used for testing the model performance. The data used in this figure were taken from ref. [75].

loss, dielectric breakdown, resistance to degradation, film formability, mechanical behavior, and integrity, etc., are relevant and cannot be ignored. Thus, the initial screening criteria adopted must be viewed as "necessary but not sufficient" conditions.

As mentioned in Section 2.2, the choices of the dielectric constant and bandgap as initial focal points were motivated by the consideration that computing these properties may be viewed as largely "solved problems" (relative to computing other relevant properties). On the other hand, several other enormously important factors such as the dielectric loss at application-relevant (ca. kHz) frequencies, morphological evolution and the progressive creation/dynamics of defects in the presence of a persistent large electric field, and dielectric breakdown are largely "unsolved" problems. That is, first-principles calculations cannot, at the moment, be used readily and accurately to estimate these properties, as they are for the bandgap and dielectric constant. The hope for continued progress and ingenuity in this field will be determined largely by new methodology developments to address these unsolved problems based on synergies between advanced characterization and materials modeling efforts.

One matter that was not discussed in this review is the emerging role of data-driven methods in further accelerating the materials-discovery process.[73] Within the context of discovery of polymer dielectrics, the community has accumulated an enormous amount of data for a variety of materials (including those that are promising, and those that are not); see, for instance, the data contained in Figure 16, which was created at a uniform level of theory. Much of the available data can be put to use going forward, via statistical or machine-learning (ML) algorithms trained on past data, in an attempt to tease out basic principles and guidelines, to make optimal choices among a myriad of possibilities that go beyond the original chemical subspace considered, and to make informed "go/no go" decisions on whether a new material should be synthesized and tested. Such predictions have indeed been attempted in the recent past for the case of both organic[74,75] and group-14-based polymers,[76] via an intermediate "fingerprinting" step wherein every polymer is represented numerically. A major advantage of these strategies is that property predictions can be made at a miniscule fraction of the cost incurred in first-principles computations or explicit experimentation, and thus the effort required in traversing vast chemical spaces may be much alleviated.

As an example, we describe here the development of an ML model[75] for the dataset of organic polymers presented in Section 2.2 and Figure 5. We fingerprinted the polymers based on the number of constituent blocks of different types and their neighbors, and mapped this fingerprint to the computed properties using a regression algorithm. A prediction model was thus trained and tested on the available dataset; a comparison of the predictions of the ML model and the DFT-computed results is shown in **Figure 17**. Given the closeness of the two, it is clear that the ML model is a suitable substitute for future DFT, and properties of any new polymers belonging to the same chemical subspace can instantly and trivially be determined without having to perform expensive DFT computations anymore. This significantly accelerates the "initial computational guidance" segment of the rational co-design approach loop, thus further improving the prospects of the design of new polymer dielectrics.

We close by re-emphasizing that the prospects for systematic, rational, and accelerated approaches toward materials discovery appear to be strong. Although the focus here was the design of polymer dielectrics for high-energy-density applications, recent successes in several other materials-discovery efforts by the community provide evidence that a cooperative computation–synthesis–processing–characterization co-design paradigm can bear fruit. This outlook is consistent with the charter of the Materials Genome Initiative, which mandates the community to surpass traditional (but valuable) Edisonian and intuition-driven approaches adopted to date.

Acknowledgements

A.M.-K. and G.T. contributed equally to this work. The authors acknowledge financial support for their high energy density capacitor materials research from the Office of Naval Research (ONR), most recently

through a multidisciplinary university research initiative (MURI) grant. Several useful discussions with Michele Anderson, Paul Armistead, Steve Boggs, Jeff Calame, and Kenny Lipkowitz are gratefully acknowledged.

Received: January 21, 2016
Revised: February 15, 2016
Published online: May 11, 2016

[1] T. P. Hughes, in *Technology at the Turning Point*, 1st ed., (Ed: P. W. Pickett), San Francisco Press, San Francisco, CA, USA, **1977**, pp. 5–22.
[2] R. D. Friedel, P. Israel, B. S. Finn, *Edison's Electric Light: Biography of an Invention*, Rutgers University Press, New Brunswick, NJ, USA **1987**.
[3] I. Takeuchi, R. B. van Dover, H. Koinuma, *MRS Bull.* **2002**, *27*, 301.
[4] H. Koinuma, H. N. Aiyera, Y. Matsumoto, *Sci. Tech. Adv. Mater.* **2000**, *1*, 1.
[5] B. Jandeleit, D. J. Schaefer, T. S. Powers, H. W. Turner, W. H. Weinberg, *Angew. Chem. Int. Ed.* **1999**, *38*, 2494.
[6] G. Ceder, K. Persson, *Sci. Am.* **2013**, *309*, 36.
[7] A. Jain, Y. Shin, K. A. Persson, *Nat. Rev. Mater.* **2016**, *1*, 15004.
[8] G. Ceder, Y.-M. Chiang, D. R. Sadoway, M. K. Aydinol, Y.-I. Jang, B. Huang, *Nature* **1998**, *392*, 694.
[9] H. Peng, A. Zakutayev, S. Lany, T. R. Paudel, M. d'Avezac, P. F. Ndione, J. D. Perkins, D. S. Ginley, A. R. Nagaraja, N. H. Perry, T. O. Mason, A. Zunger, *Adv. Funct. Mater.* **2013**, *42*, 5267.
[10] R. Gautier, X. Zhang, L. Hu, L. Yu, Y. Lin, T. O. L. Sunde, D. Chon, K. R. Poeppelmeier, A. Zunger, *Nat. Chem.* **2015**, *7*, 308.
[11] B. Balke, S. Wurmehl, G. H. Fecher, C. Felser, J. Kübler, *Sci. Technol. Adv. Mater.* **2008**, *9*, 014102.
[12] J. K. Nørskov, T. Bligaard, J. Rossmeis, C. H. Christensen, *Nat. Chem.* **2009**, *1*, 37.
[13] V. Sharma, C. C. Wang, R. G. Lorenzini, R. Ma, Q. Zhu, D. W. Sinkovits, G. Pilania, A. R. Oganov, S. Kumar, G. A. Sotzing, S. A. Boggs, R. Ramprasad, *Nat. Commun.* **2014**, *5*, 4845.
[14] R. Ma, A. F. Baldwin, C. C. Wang, I. Offenbach, M. Cakmak, R. Ramprasad, G. A. Sotzing, *ACS Appl. Mater. Interfaces* **2014**, *6*, 10445.
[15] R. G. Lorenzini, W.M. Kline, C. C. Wang, R. Ramprasad, G. A. Sotzing, *Polymer* **2013**, *54*, 3529.
[16] A. F. Baldwin, R. Ma, A. Mannodi-Kanakkithodi, T. D. Huan, C. C. Wang, M. Tefferi, J. E. Marszalek, M. Cakmak, Y. Cao, R. Ramprasad, G. A. Sotzing, *Adv. Mater.* **2015**, *27*, 346.
[17] A. F. Baldwin, T. D. Huan, R. Ma, A. Mannodi-Kanakkithodi, M. Tefferi, N. Katz, Y. Cao, R. Ramprasad, G. A. Sotzing, *Macromolecules* **2015**, *48*, 2422.
[18] A. F. Baldwin, R. Ma, T. D. Huan, Y. Cao, R. Ramprasad, G. A. Sotzing, *Macromol. Rapid Commun.* **2014**, *35*, 2082.
[19] Materials Genome Initiative (MGI) (**2011**), https://www.whitehouse.gov/mgi; accessed: September 2015.
[20] J. J. de Pablo, B. Jones, C. L. Kovacs, V. Ozoliņš, A. P. Ramirez, *Curr. Opin. Solid State Mater. Sci.* **2014**, *18*, 99.
[21] *Integrated Computational Materials Engineering: A Transformational Discipline for Improved Competitiveness and National Security*, The National Academies Press, Washington DC, USA **2008**.
[22] A. Jain, S. P. Ong, G. Hautier, W. Chen, W. D. Dacek, S. Richards, S. Cholia, D. Gunter, D. Skinner, G. Ceder, K. A. Persson, *APL Mater.* **2013**, *1*, 011002.
[23] R. H. Taylor, F. Rose, C. Toher, O. Levy, K. Yang, M. B. Nardelli, S. Curtarolo, *Comput. Mater. Sci.* **2014**, *93*, 178.
[24] J. E. Saal, S. Kirklin, M. Aykol, B. Meredig, C. Wolverton, *JOM* **2013**, *65*, 1501.
[25] A. Belsky, M. Hellenbrandt, V. L. Karen, P. Luksch, *Acta Crystallogr.* **2002**, *B58*, 364.
[26] Khazana, http://khazana.uconn.edu/; accessed: October 2015.
[27] *Handbook of Low and High Dielectric Constant Materials and Their Applications*, (Ed: H. S. Nalwa), Academic Press **1999**.
[28] J. B. Ennis, F. W. MacDougall, X. H. Yang, R. A. Cooper, K. Seal, C. Naruo, B. Spinks, P. Kroessler, J. Bates, *16th IEEE Int. Pulsed Power Conf*, IEEE, Piscataway, NJ, USA, **2007**, 282.
[29] F. Ennis, J. MacDougall, X. H. Yang, R. A. Cooper, J. E. Gilbert, J. F. Bates, C. Naruo, M. Schneider, N. Keller, S. Joshi, T. R. Jow, J. Ho, C. J. Scozzie, S. P. S. Yen, in *IEEE Pulsed Power Conf.*, IEEE, Piscataway, NJ, USA **2009**, p. 774.
[30] H. Bluhm, *Pulsed Power Systems: Principles and Applications*. Springer Verlag, Berlin/Heidelberg, Germany **2006**.
[31] L. Yang, J. Ho, E. Allahyarov, R. Mu, L. Zhu, *ACS Appl. Mater. Interfaces.* **2015**, *7*, 19894.
[32] Q. M. Zhang, V. Bharti, X. Zhao, *Science* **1998**, *280*, 2101.
[33] B. Chu, X. Zhou, K. Ren, B. Neese, M. Lin, Q. Wang, F. Bauer, Q. M. Zhang, *Science.* **2006**, *313*, 334.
[34] W. Li, L. Jiang, X. Zhang, Y. Shen, C. W. Nan, *J. Mater. Chem. A.* **2014**, *2*, 15803.
[35] L. Jiang, W. Li, J. Zhu, X. Huo, L Luo, Y. Zhu, *Appl. Phys. Lett.* **2015**, *106*, 052901.
[36] S. Zhang, C. Zou, D. I. Kushner, X. Zhou, R. J. Orchard, N. Zhang, Q. M. Zhang, *IEEE Trans. Dielectr. Electr. Insul.* **2012**, *19*, 1158.
[37] M. R. Gadinski, K. Han, Q. Li, G. Zhang, W. Reainthippayasakul, Q. Wang, *ACS Appl. Mater. Interfaces.* **2014**, *6*, 18981.
[38] Y. Shen, Y. Lin, Q. M. Zhang, *MRS Bull.* **2015**, *40*, 433.
[39] A. L. An, S. A. Boggs, in *Conf. Record 2006 IEEE International Symposium on Electrical Insulation, IEEE*, Piscataway, NJ, USA **2006**, p. 273.
[40] L. An, S. A. Boggs, J. P. Calame, in *Proc. 2008 IEEE International Power Modulators and High Voltage Conf., IEEE*, Piscataway, NJ, USA **2008**, p. 552.
[41] J. M. Carr, M. Mackey, L. Flandin, D. Schuele, L. Zhu, E. Baer, *J. Polym. Sci., Part B: Polym. Phys.* **2013**, *51*, 882.
[42] Z. Zhou, J. Carr, M. Mackey, K Yin, D. Schuele, L. Baer, E. Zhu, *J. Polym. Sci., Part B: Polym. Phys.* **2013**, *51*, 978.
[43] M. A. Wolak, M.-J. Pan, A. Wan, J. S. Shirk, M. Mackey, A. Hiltner, E. Baer, L. Flandin, *Appl. Phys. Lett.* **2008**, *92*, 113301.
[44] J. K. Tseng, S. Tang, Z. Zhou, M. Mackey, J. M. Carr, R. Mu, L. Flandin, D. E. Schuele, E. Baer, L. Zhu, *Polymer* **2014**, *55*, 8.
[45] M. Mackey, D. E. Schuele, L. Zhu, L. Flandin, M. A. Wolak, J. S. Shirk, A. Hiltner, E. Baer, *Macromolecules* **2012**, *45*, 1954.
[46] T. D. Huan, S. Boggs, G. Teyssedre, C. Laurent, M. Cakmak, S. Kumar, R. Ramprasad, *Prog. Mater. Sci.*, DOI: 10.1016/j.pmatsci.2016.05.001.
[47] C. C. Wang, G. Pilanina, S. Boggs, S. Kumar, C. Breneman, R. Ramprasad, *Polymer* **2014**, *55*, 979.
[48] P. Hohenberg, W. Kohn, *Phys. Rev. B.* **1964**, *136*, 864.
[49] W. Kohn, L. J. Sham, *Phys. Rev. A.* **1965**, *140*, 1133.
[50] S. Baroni, S. de Gironcoli, A. Dal Corso, P. Giannozzi, *Rev. Mod. Phys.* **2001**, *73*, 515.
[51] J. McPherson, J. Kim, A. Shanware, H. Mogul, J. Rodriguez, *Tech. Dig. Int. Electron Devices Meet.* **2002**, *2002*, 633.
[52] J. Heyd, G. E. Scuseria, M. Ernzerhof, *J. Chem. Phys.* **2003**, *118*, 8207.
[53] J. P. Perdew, *Int. J. Quant. Chem.* **1985**, *28*, 497.
[54] C. C. Wang, G. Pilania, R. Ramprasad, *Phys. Rev. B.* **2013**, *87*, 035103.
[55] Q. Zhu, A. R. Oganov, C. W. Glass, H. T. Stokes, *Acta Crystallogr.* **2012**, *B68*, 215.
[56] Q. Zhu, V. Sharma, A. R. Oganov, R. Ramprasad, *J. Chem. Phys.* **2014**, *141*, 154102.
[57] R. Ma, V. Sharma, A. F. Baldwin, M. Tefferi, I. Offenbach, M. Cakmak, R. Weiss, Y. Cao, R. Ramprasad, G. A. Sotzing, *J. Mater. Chem. A.* **2015**, *3*, 14845.
[58] S. Wu, W. Li, M. Lin, Q. Burlingame, Q. Chen, A. Payzant, K. Xiao, Q. M. Zhang, *Adv. Mater.* **2013**, *25*, 1734.

[59] H. Fujiwara, in *Handbook of Optical Metrology: Principles and Applications, 2nd Ed*., CRC Press, Boca Raton, FL, USA **2009**, p. 641.
[60] J. O. Simpson, A. K. St. Clair, *Thin Solid Films* **1997**, *308–309*, 480.
[61] H. J. Hwang, C.H. Li, C. S. Wang, *Polymer* **2006**, *47*, 1291.
[62] A. M. North, J. C. Reid, *Eur. Polym. J.* **1972**, *8*, 1129.
[63] T. D. Huan, A. Mannodi-Kanakkithodi, C. Kim, V. Sharma, G. Pilania, R. Ramprasad, *Sci. Data* **2016**, *3*, 160012.
[64] G. Pilania, C. C. Wang, K. Wu, N. Sukumar, C. Breneman, G. Sotzing, R. Ramprasad, *J. Chem. Inf. Model.* **2013**, *53*, 879.
[65] A. Mannodi-Kanakkithodi, C. C. Wang, R. Ramprasad, *J. Mater. Sci.* **2015**, *50*, 801.
[66] C. E. Carraher Jr., M. R. Roner, *J. Organomet. Chem.* **2014**, *751*, 67.
[67] Q. Li, L. Chen, M. R. Gadinski, S. Zhang, G. Zhang, H. Li, A. Haque, L. Q. Chen, T. Jackson, Q. Wang, *Nature* **2015**, *523*, 576.
[68] A. F. Baldwin, R. Ma, C. C. Wang, R. Ramprasad, G. A. Sotzing, *J. Appl. Polym. Sci.* **2013**, *130*, 1276.
[69] S. Goedecker, *J. Chem. Phys.* **2004**, *120*, 9911.
[70] M. Amsler, S. Goedecker, *J. Chem. Phys.* **2010**, *133*, 224104.
[71] J. P. Perdew, K. Burke, M. Ernzerhof, *Phys. Rev. Lett.* **1996**, *77*, 3865.
[72] X. Xiao, X. Han, Z. Mei, D. Zhu, K. Shao, J. Liang, M. Tian, L. Xu, *J. Organomet. Chem.* **2013**, *729*, 28.
[73] T. Mueller, A. G. Kusne, R. Ramprasad, in *Reviews in Computational Chemistry*, (Eds: L. A. Parrill, B. K. Lipkowitz), Wiley, New York **2016**.
[74] T. D. Huan, A. Mannodi-Kanakkithodi, R. Ramprasad, *Phys. Rev. B.* **2015**, *92*, 014106.
[75] A. Mannodi-Kanakkithodi, G. Pilania, T. D. Huan, T. Ramprasad, R. Lookman, *Sci. Rep.* **2016**, *6*, 20952.
[76] G. Pilania, C. C. Wang, X. Jiang, S. Rajasekaran, R. Ramprasad, *Sci. Rep.* **2013**, *3*, 2810.